Modeling the Self-Assembly of Lipids and Nanotubes in Solution: Forming Vesicles and Bicelles with Transmembrane Nanotube Channels

Meenakshi Dutt, Olga Kuksenok, Michael J. Nayhouse, Steven R. Little, and Anna C. Balazs*

Chemical Engineering Department, University of Pittsburgh, Pittsburgh, Pennsylvania 15261, United States

ABSTRACT *Via* dissipative particle dynamics (DPD), we simulate the self-assembly of end-functionalized, amphiphilic nanotubes and lipids in a hydrophilic solvent. Each nanotube encompasses a hydrophobic stalk and two hydrophilic ends, which are functionalized with end-tethered chains. With a relatively low number of the nanotubes in solution, the components self-assemble into stable lipid−nanotube vesicles. As the number of nanotubes is increased, the system exhibits a vesicle-to-bicelle transition, resulting in stable hybrid bicelle. Moreover, our results reveal that the nanotubes cluster into distinct tripod-like structures within the vesicles and aggregate into a ring-like assembly within the bicelles. For both the vesicles and bicelles, the nanotubes assume trans-membrane orientations, with the tethered hairs extending into the surrounding solution or the encapsulated fluid. Thus, the hairs provide a means of regulating the transport of species through the self-assembled structures. Our findings provide guidelines for creating nanotube clusters with distinctive morphologies that might be difficult to achieve through more conventional means. The results also yield design rules for creating synthetic cell-like objects or microreactors that can exhibit biomimetic functionality.

KEYWORDS: hybrid vesicle · bicelle · self-assembly · lipids · end-functionalized nanotubes

One of the grand challenges confronting both the physical and biological sciences is the fabrication of "artificial cells" from purely synthetic components. Natural cells are powerful microreactors that involve the controlled uptake and release of vital components. Within the cell membrane, protein channels serve to actively regulate the traffic through the cell; one of the essential tasks in creating a synthetic cell is designing channels that could perform a similar regulatory function. A possible route for forming a cell-like object that contains functional channels is through the self-assembly of lipids and "hairy" nanotubes (NTs), which are decorated with polymer chains at both ends. Under the appropriate conditions, these components could potentially self-organize into a hybrid structure, with the lipids forming a vesicle and the nanotubes spanning the vesicle's membrane. In this configuration, the hairs on the nanotubes' ends could be harnessed to filter the motion of species in and out of the vesicle and the entire structure could be utilized to fabricate biomimetic, small-scale reactors. Additionally, these assemblies could be harnessed as controlled release devices, with the hairs providing a means of regulating the release of the encapsulated species.

In this paper, we use computational modeling to isolate regions of parameter space where mixtures of lipids and hairy nanotubes in an aqueous solution can spontaneously self-assemble into vesicles with membrane-spanning channels. An example of this structure is shown in Figure 1. Here, the hydrophobic shafts of the nanotubes are embedded in the membrane and the hydrophilic hairs extend into the external solution and the interior of the vesicle, providing a means of reversibly closing or opening these pores (*e.g.*, through a change in solvent quality or pH).[1] Notably, the nanotubes have associated into a tripod-like structure; as we show below, this configuration is quite robust and can be obtained reproducibly. Hence, the vesicles provide a "reaction chamber" for creating nanoparticles with distinctive morphologies[2,3] that might be difficult to achieve through more conventional means.

A number of recent studies have focused on the self-assembly of lipids in solution,[4−24] allowing researchers to identify the salient features of this process. Significant progress has also been made in understanding the dynamic behavior of preassembled, multicomponent lipid vesicles.[25−29] Despite the significant interest in harnessing nanotubes for biomedical applications, the self-assembly of dispersed lipid molecules and nanotubes

* Address correspondence to balazs@pitt.edu.

Received for review February 23, 2011 and accepted May 23, 2011.

Published online May 23, 2011
10.1021/nn201260r

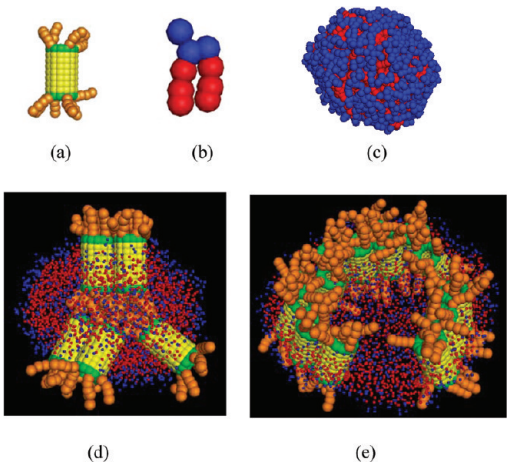

Figure 1. (a,b) Schematic of an amphiphilic NT (a) and coarse-grained model of a twin-tailed lipid (b). (c−e) Examples of self-assembled structures: (c) vesicle self-assembled from amphiphilic lipids dispersed in a hydrophilic solvent, (d) lipid-NT hybrid vesicle (413 lipids and 7 NTs), and (e) lipid-NT hybrid bicelle (270 lipids and 18 NTs). The lipid head and tail bead radii have been reduced to one-fourth of their original values to more clearly reveal the NT organization in panels d and e. Here and in all the images below, the solvent beads are not shown.

has not been extensively explored. To the best of our knowledge, the simulations presented herein constitute the first studies of the association of the lipids and nanotubes into vesicles. To probe the structure formation, we systematically increased the fraction of nanotubes in the solution and thereby uncovered a novel vesicle to bicelle transition. These hybrid lipid/nanotube bicelles are stable structures, and consequently, they too could be used as reaction chambers. On a fundamental level, the emergence of the bicelles provides insight into the factors that control the organization of lipid−nanotube assemblies.

In contrast to the dearth of investigations on lipid/nanotube vesicles, there have been a number of computational studies on the interactions of cylindrical inclusions and preassembled lipid membranes.[30−46] Recently, we simulated the behavior of hairy nanotubes, with hydrophilic hairs at one or both ends, in the presence of preassembled "flat" membranes.[47] We found that nanotubes with hairs at just one end could spontaneously insert into the membrane. For nanotubes with hairs at both ends, however, the membrane had to be perforated in order to trap these nanoparticles within the bilayer. On the basis of these findings, we now examine how self-assembly can be exploited to spontaneously integrate nanotubes with hairs at both ends into the bilayer of a vesicle, and thus, in one step create a cell-like structure with the biomimetic channels.

It is worth noting that there have been few experimental studies involving the self-assembly of short nanotubes and lipid molecules; a stumbling block is creating nanotubes that are comparable in length to the lipids. Researchers are, however, making significant progress toward this end. For example, techniques such as fluorination[48] and freezing and cutting[49] have been used to obtain ultrashort (US) single-walled carbon nanotubes (SWCNT) of lengths 50 nm or less. In addition, A. Javey *et al*. used a combination of photolithography and shadow evaporation to fabricate a device composed of US-SWCNT that are 10 nm in length.[50] Recently, researchers have fabricated US-SWCNT that are on average approximately 7.5 nm in length (with the shortest nanotubes being 2 nm) through the use of density gradient ultracentrifugation.[51] Hence, the average size of the latter nanotubes is just a factor of 2 longer than the nanotubes considered herein (with the shortest nanotubes being on the same length scale as those in our studies).

In the ensuing studies, we also assume that the nanotubes are end-functionalized and such modes of functionalization can be readily achieved experimentally. For instance, carbon nanotubes can be functionalized through thermal activation, electrochemical modification, or photochemical reactions.[52] K. M. Lee *et al*. demonstrated the asymmetric end-functionalization of multiwall carbon nanotubes using hydrophilic and hydrophobic moieties.[53] J.J. Stephenson *et al*. and others have functionalized US-SWCNTs using various moieties both on its ends and side walls.[54−58] Thus, with the fabrication of the appropriate ultrashort nanotubes, the chemical functionalization described herein can be realized.

In carrying out these studies, we use dissipative particle dynamics (DPD) simulations. The DPD is essentially a coarse-grained molecular dynamics (MD) method, allowing researchers to examine larger systems in more computationally realistic time frames.[59] The technique has proven to be especially useful in studying the mesoscale behavior of bilayer membranes.[4,25,26,30,59−64] We provide a brief description of the DPD simulations in the Methodology section.

RESULTS AND DISCUSSIONS

The basic structural units in our system are the amphiphilic, hairy nanotubes and the twin-tailed lipids shown in Figure 1 panels a and b, respectively. As detailed in the Methodology, each nanotube encompasses a hydrophobic stalk, which is capped by a single band of hydrophilic beads at both top and bottom. Hydrophilic hairs are tethered to both ends of these nanotubes (see Figure 1a). At the onset, we randomly distribute a mixture of the hairy nanotubes, lipids, and hydrophilic solvent beads in a simulation box that is 30 $\times$ 30 $\times$ 30 r_c^3 units in size, where $r_c = 1$ is the interaction distance (see Methodology); the total number of beads is fixed at 81000. We vary the number of the NTs (from 0 to 18) while keeping the total fraction of amphiphilic species fixed at 5.6% of the beads in the simulation box.[65]

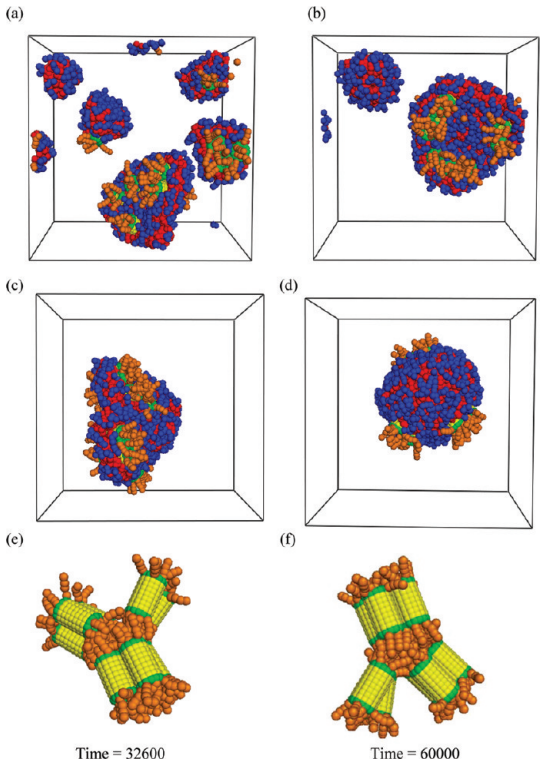

Figure 2. (a−d) Snapshots of the system with 10 NTs (and 374 lipids) during the self-assembly process for times (a) 3300, (b) 5200, (c) 8900, and (d) 32600. (e−f) Snapshots of the NT organization at times (e) 32600 and (f) 60000 (lipid beads are not shown). The dimensionless time is measured in units of τ (see Methodology). To visualize the dynamics of the self-assembly process, see movies SI.001 and SI.002 in Supporting Information.

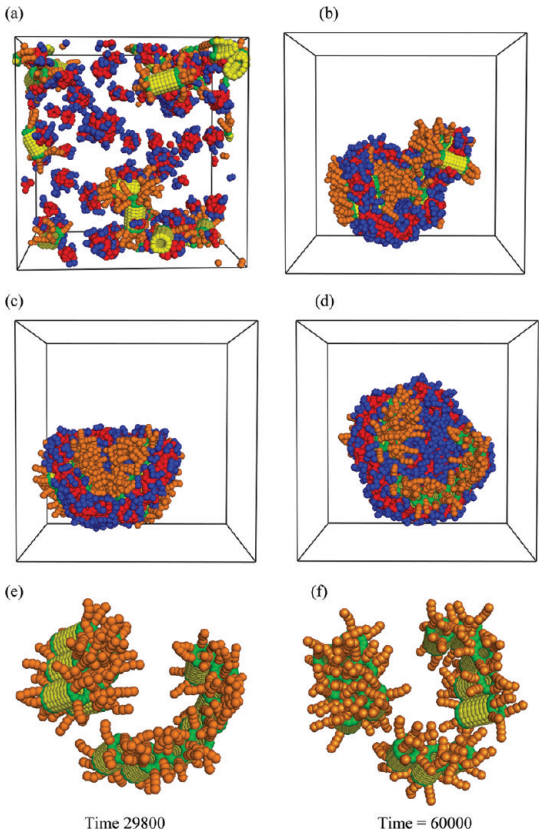

Figure 3. Snapshots of the system with 14 NTs (and 322 lipids) during the self-assembly process for times (a) 200, (b) 22800, (c) 23800, and (d) 29800. Snapshots of the NT organization at times (e) 29800 and (f) 60000 (lipid beads are not shown). To visualize the dynamics of the self-assembly process, see movie SI.003 in Supporting Information.

In the absence of NTs, we observe the formation of stable lipid vesicles (see Figure 1c), in agreement with previous studies involving the self-assembly of similar lipids at comparable concentrations.[4] As we show below, the introduction of amphiphilic NTs affects not only the morphology of the self-assembled structures, but also the dynamics of the self-assembly process. Depending on the fraction of NTs in the solution, our results reveal two distinct scenarios. In the first scenario, the mixture forms a lipid−NT vesicle, with small clusters of nanotubes being embedded in the vesicle's membrane (see Figures 1d and 2). The second scenario occurs at higher fractions of NTs: the system associates into a hybrid bicelle structure, with large clusters of NTs (or a single cluster) forming a ring-like structure close to the edges of the bicelle (see Figures 1e and 3). For a given NT concentration, we performed multiple independent simulations and found these morphologies to be highly robust. Below, we first focus on specific samples that exemplify the self-assembly of the hybrid vesicles and bicelles. We then describe aggregate properties of the system that are obtained by systematically varying the number of nanotubes and averaging the data over eight independent runs.

To illustrate the self-assembly of hybrid vesicles, we randomly distribute a mixture of 10 NTs, 374 lipid molecules and hydrophilic solvent beads in our simulation box (so that the total volume fraction of the amphiphilic beads is fixed at 5.6%). The structural evolution of this system is shown in Figure 2 (see corresponding movie SI.001 in Supporting Information). At early times, some of the lipids aggregate into the small micelles,[4,66,67] while other lipids coat the NTs to minimize the unfavorable shaft−solvent interactions. These small lipid micelles and lipid-coated NTs merge to form larger assemblies, including bicelles (Figure 2a). In the transient, hybrid bicelles, the hydrophobic shafts of the nanotubes are shielded from the solvent by the lipid tails or other nanotubes, and the tethered hydrophilic hairs extend into the solution (much as in the larger structure in Figure 1e). The aggregation process continues until all the amphiphilic species form a single hybrid bicelle (Figure 2c); notably, the NTs form relatively large clusters located close to the edge of the bicelle. As can be seen in Figure 2c, some of the hydrophobic tails are exposed to the aqueous solution at the periphery of the bicelle. To alleviate these energetically unfavorable interactions,

this transient bicelle effectively folds on itself and merges all its edges. Consequently, the system forms a relatively spherical vesicle (see Figure 2d and the corresponding movie SI.002 in the Supporting Information) that encloses hydrophilic solvent and the hydrophilic hairs (which emanated from the inner curved surface). It is worth noting that the enclosed hydrophilic hairs occupy approximately 70% of the total volume inside the vesicle shown in Figure 2d.

For self-assembled amphiphilic lipids in the absence of nanotubes, the transition from the bicelles (also referred to as a disk-like micelles or bilayers) to vesicles has been investigated by a number of researchers.[4,14−16,22−24,68−70] The theoretical model developed by Fromherz[68,69] describes the bilayer-to-vesicle transition in terms of minimizing the sum of the edge and bending energies. As the bicelle folds to form the vesicle, the edge energy is decreased, but correspondingly, the bending energy is increased. The transition becomes energetically favorable when the bicelle reaches a certain critical size, which depends on the bending rigidity of the bilayers.[68,69] These observations were later corroborated in a number of computer simulations.[16,66,67,72] In addition, recent coarse-grained molecular dynamic studies[70] have highlighted the role of entropic effects in the bicelle-to-vesicle transition.[71] A number of experimental studies[14,15,22−24] have confirmed the formation of lipid vesicles through the folding of transient bicelles that reached a critical size.

For the system shown in Figure 2, we observe that the bicelle-to-vesicle transition occurs in a qualitatively similar manner as in the lipid/solvent mixture (no NTs).[4−9,12,66−70] The self-assembly of the components results in the formation of a stable hybrid vesicle with nanotubes positioned in a transmembrane configuration and hydrophilic tethers exposed to the solvent inside the vesicle cavity and external solution (see Figure 2d). Figure 2 panels e and f show the late time organization of the NTs within the vesicle; for clarity, the lipid beads are not displayed. Figure 2e corresponds to the same simulation time as Figure 2d, while Figure 2f shows the NT distribution at much later times. The images in Figure 2 panels e and f reveal that the relative organization of the clusters remains stable over the long time dynamics of the system. Within each of the three clusters shown in Figure 2e,f, the NTs are oriented approximately parallel to each other (with some fluctuations in the relative organization of the nanotubes within a given cluster). We emphasize the robustness of the dynamics illustrated in Figure 2: in all eight independent runs with 10 NTs, the vesicle is found to have two to three nanotube clusters, with each cluster containing approximately two to five nanotubes. (We note that three clusters are observed in the seven of the eight runs at the late time $t = 6 \times 10^4$).

When the number of end-functionalized NTs is increased to 14 (and the solution contains 322 lipid molecules), we find that the system forms a stable hybrid bicelle, with nanotubes in a transmembrane configuration and the hydrophilic tethers extending into the solvent. The structural evolution of this system is depicted in Figure 3. The smaller aggregates formed during the initial stages of the self-assembly continue to merge to form larger structures, including bicelles (Figure 3a). In some cases, we observe a curved bicelle to unfold after fusion with a micelle, or a smaller bicelle (see Figure 3b). The end-functionalized nanotubes reorganize to lie near the aggregate edges, and the bicelle is observed to fold again. This aggregation process continues until a single bicelle is formed; this large bicelle curves into a transient cup-shaped structure (see Figure 3c). The aggregate in Figure 3c appears to be attempting to fuse its edges (similar to the case of 10 NTs); during this process, the end-functionalized nanotubes diffuse to the edges of the aggregate. The dynamics of this process can be seen in the corresponding Supporting Information movie SI.003. For this high fraction of the NTs, we do not observe the fusion of the bicelle edges and the formation of the vesicle; rather, the nanostructured bicelle morphology remains stable (see Figure 3d). The nanotubes self-organize into clusters arranged in a ring-like configuration (Figure 3e,f). Near the edge of the bicelle, the lipids rearrange to minimize the contact between the hydrophobic moieties and the hydrophilic solvent. In particular, the lipid head groups point toward the solvent, forming a curved, hydrophilic outer layer (Figure 3d).

We hypothesize that the stability of the bicelle in this case (and the inability of the system to form a vesicle) could be the result of the following factors. First, in order for the vesicle to form, the hydrophilic hairs must be accommodated within the interior of the spherical structure. For the vesicle with 10 NTs, the hairs already occupied approximately 70% of the interior space. At 14 NTs, an even higher concentration of hairs would need to be localized inside the vesicle; this type of confinement could be entropically unfavorable. Second, the addition of the rigid NTs increases the bending modulus of the bilayer. As shown earlier for lipid/solvent systems,[23,42,66−69] during the bicelle-to-vesicle transitions, the bicelle folds to merge its edges. Because of the relatively low bending modulus of the lipid membrane, the increase in the bending energy is compensated by the decrease in the edge energy. In our simulation, the bending modulus of the pure lipid membrane (no NTs) is also low (as described in the Methodology, the lipid tails are highly flexible). As we add rigid NTs, however, we effectively increase the membrane stiffness. Hence, we hypothesize that increasing the bending rigidity of the membrane by adding a higher fraction of the NTs could effectively prevent the bicelle-to-vesicle transition and stabilize the hybrid bicelle.

To probe the effects of the above factors on the self-assembly shown in Figure 3, we conducted the following studies. First, to elucidate the role of the hydrophilic hairs, we ran simulations with 14 "hairless" NTs, which did not encompass the tethered chains at ends of the shafts; all other parameters were identical to those noted in Figure 3. Our results showed that the self-assembly process and the late-time, stable bicelle structure remains essentially the same as in the case of the hairy NTs (see Figure S4 in the Supporting Information). Hence, the hairs are not responsible for precluding the bicelle-to-vesicle transition.

Next, we investigated the effect of the membrane's bending rigidity. The bending rigidity can be increased by either increasing the volume fraction of the rigid inclusions (in which case, the bending modulus of the membrane would vary locally), or increasing the stiffness of the lipids by introducing an angle-dependent potential[73,74] between contiguous beads in the tails. Here, we use a three-body stiffness potential of the form $E_{angle} = K_{angle}(1 + \cos\theta)$ where θ is the angle formed by three adjacent beads.[73,74] With this modification, we obtained the self-assembled morphologies for lipids in solution (no NTs) for $K_{angle} = 5$, 10, 15, and 20. Our simulations show that the stable, self-assembled morphology is a bicelle for $K_{angle} = 20$, and a vesicle for lower values of K_{angle} (K_{angle} = 5, 10, 15). (Similar results were shown in earlier simulations for lipid-solvent systems.[70]) We then set $K_{angle} = 10$, and studied mixtures of amphiphilic lipids and different numbers of the end-functionalized nanotubes in the aqueous solution. The NTs are the same as shown in Figure 1a, and the total concentration of amphiphilic beads (lipids and NTs) is kept fixed at 5.6%. We found that only the system with one nanotube formed a stable vesicle, whereas systems with larger fractions of nanotubes formed stable bicelles. The same results were obtained for eight independent runs

The above observations indicate that an increase in the bending rigidity of the aggregate (achieved either through the addition of a sufficient number of NTs or by increasing the rigidity of the lipids or by a combination of both factors) drives the transition from a vesicle to a bicelle.[75] In other words, our simulations provide the first evidence that an increase of the fraction of the NTs prevents the late time bicelle-to-vesicle transition and yields a stable, hybrid bicelle as a result of the self-assembly process.

As was previously observed for lipids in solvents without nanotubes,[4,16,66,67] the self-assembly illustrated in Figures 2 and 3 minimizes the total energy of the mixture (see black and red curves in Figure 4a for the respective cases shown in Figures 2 and 3). The points on the curves correspond to the indicated snapshots in Figures 2 and 3. In these plots, the total energy consists of the following:[59,62,73] the pair interaction energy between all the beads in the system, the bond energy of the harmonic springs within the lipids and chains tethered to the NTs, and a three-body stiffness potential within the tethered chains. (It is important to remind the reader that the magnitude of the pair interaction between the DPD beads is directly related to the solubility of the respective species. In effect, the DPD pair interaction energy is directly related to the Flory–Huggins energy of immiscible polymer blends.[59] For more details, see ref 58 and Methodology section). We observe a significant decrease in this energy during the early to intermediate times, when the components are assembling into a single hybrid aggregate. On the other hand, the total energy during late times, when the vesicle or bicelle is undergoing a restructuring, remains approximately constant (within the range of the fluctuations). We also plotted the evolution of all the energy components (see S4–S6 in Supporting Information); the plots reveal that a decrease in the total energy is mostly due to the decrease in the pair interaction energy between the hydrophobic and hydrophilic beads (as was observed for the purely lipid system[4]). The minimization of the total energy of the system during the self-assembly process seen in Figure 4a is also observed in all the eight independent simulations. In the Supporting Information (S7), we provide the plot of the total energy averaged over the eight independent runs for the case of vesicle formation with 10 NTs. This plot confirms the features highlighted above; namely, it illustrates a significant decrease in energy during the assembly process into a single hybrid aggregate and shows that the actual decrease in energy during the bicelle-to-vesicle transition is relatively constant within the range of fluctuations.

The images in Figures 2 and 3 show that the NTs within the assemblies organize into the well-defined structures. There are three distinct features of the NT organization that are common to both the stable vesicles and bicelles described above: (1) the NTs self-organize into large clusters; (2) NTs preferentially orient parallel to each other within a given cluster, and (3) NT clusters assume trans-membrane positions within each of the configurations, with the hairs extending into the solvent.

While our simulations provide the first examples of systems that entail all three events, some of these features have been observed in previous studies. For instance, the clustering of self-assembling amphiphilic rods, as well as the preferential parallel orientation of the rods within a cluster (resulting in the formation of liquid crystalline phases), was observed for hairy rods in solution in the absence of lipids.[77,78] Studies on rigid inclusions interacting within preassembled lipid membranes[31,33,35–37,40–43] have also demonstrated that the inclusions associate into distinct clusters. There are number of factors controlling the interactions between these rigid inclusions; among these

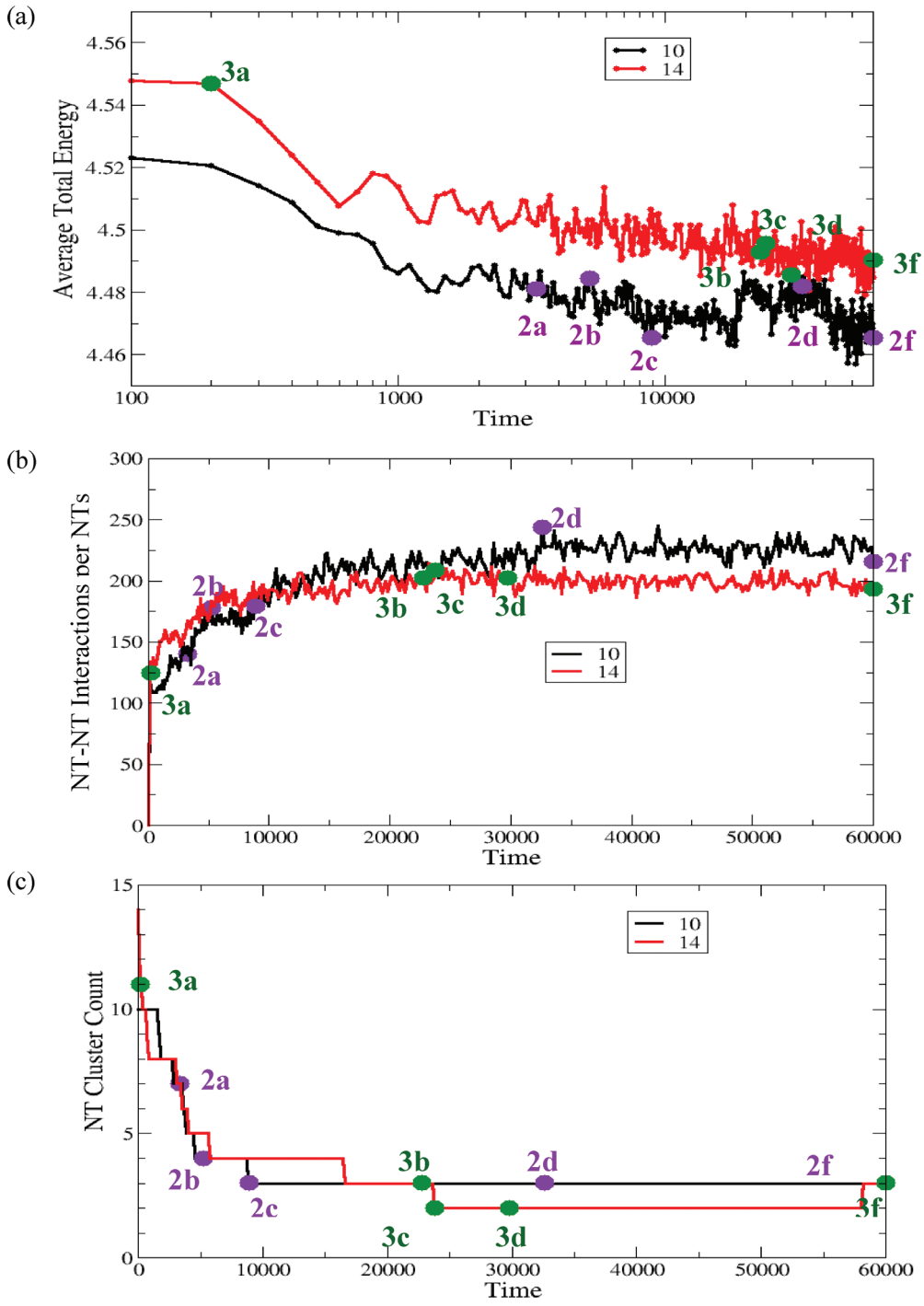

Figure 4. Time evolution of (a) the total energy per bead, (b) the NT−NT interaction count per number of NTs in the system, and (c) the NT cluster count for systems with 10 NTs (374 lipids) and 14 NTs (322 lipids). The data corresponds to systems shown in Figures 2 and 3. The data points that correspond to the snapshots in Figure 2 panels a−f and Figure 3 panels a−f are labeled as 2a−2f and 3a−3f, respectively.

factors are a hydrophobic mismatch, the packing density of the lipids around the inclusions, and a depletion attraction between the inclusions.[31,33,35−37,40−43] For our systems, we can rule out the effect of hydrophobic mismatch since the NT length is comparable to the membrane thickness (see Methodology). On the other hand, we hypothesize that depletion attraction plays an important role in the clustering of the NTs during the self-assembly of the vesicles and bicelles seen in Figures 2 and 3. Below, we isolate factors that affect the formation of the NT clusters within these self-organizing hybrid aggregates.

We quantify the interaction between the nanotubes through the "interaction count" or the number of interactions between pairs of sites on two nanotubes that are separated by a distance less than r_c. The sites

include the hydrophobic beads in the shaft, the hydrophilic beads at the ends of the shaft, and the hydrophilic beads in the tethered hairs. We compute the nanotube−nanotube interaction count in a given system from the beginning of the self-assembly process and normalize this value by the number of nanotubes. The interaction counts for the systems in Figures 2 and 3 are given in Figure 4b. The plot shows that, as could be anticipated, at early to intermediate times, the nanotube−nanotube interaction count increases with time as the nanotubes cluster within the lipid aggregates. At late times, however, the interaction count per nanotube is observed to saturate and fluctuate around a steady-state value. Hence, at late times, the number of neighboring NTs remains approximately constant.

To further characterize the self-organization of the nanotubes, we calculate the number of nanotube clusters during the course of the simulation for the cases shown in Figures 2 and 3. Here, we define a NT cluster as the number of nanotubes that are effectively "in contact", that is, each pair of NTs within the cluster have at least one interaction count where a bead within the shaft of one NT is separated by a distance $d \leq r_c$ from a bead within the shaft of another NT. (We do not consider interactions between the tethered hairs when calculating the NT clusters and the NT cluster is distinctly different from the cluster of amphiphilic species).

At the onset of the simulation, all the NTs are randomly distributed in the solution; at this stage, the number of NT clusters is just equal to the number of NTs in the system. As the NTs begin to aggregate, the total number of NT clusters, k, decreases in a stepwise manner (see Figure 4c). Typically, the NTs within a cluster are oriented approximately parallel to each other, so that there is a high interaction count per nanotube within the cluster (as can be anticipated from the data in Figure 4b). The formation of $k = 3$ distinct NT clusters is clearly evident in Figure 2 panels e and f. Similarly, Figure 3 panels e and f show two and three large NT clusters, respectively. The latter clusters form a "broken necklace" pattern, which is located close to the bicelle edges.

Figure 4c clearly illustrates that after the NTs have formed three distinct clusters within the vesicle, these clusters remain stable (see black curve for 10 NTs). For the case of the 14 NTs, however, we observe the formation of either two or three NT clusters (see red line in Figure 4c and the respective images in Figure 3 panel e and f). These late-time fluctuations between the two and three NT clusters within the bicelle do not change the interaction count and the average energy; both values remain constant within the range of fluctuations, as can be seen from the respective points in Figure 4a,b.

Up to this point, we have described two examples of different hybrid structures formed by the self-assembly of lipids and hairy nanotubes in solution. Our results indicate that this self-assembly process provides a viable approach for creating two types of distinctly different hairy NT/lipid structures. It is important to note that we carried out additional simulations on systems involving lipids and bare (nonfunctionalized) amphiphilic nanotubes and found that the major features of the self-assembly process are similar to those presented herein. For example, in a mixture of 10 bare NTs and lipids, the self-assembly process yields a stable vesicle with a few (three in the majority of the cases) clusters of bare NTs (see Supporting Information, Figure S4.a), while the self-assembly of a mixture of 14 bare NTs and lipids yields a stable bicelle (see Figure S4.b). Additional simulations showed that all of the features of the late-time NT organization within the hybrid structures discussed above are similar for bare NTs (namely, the NTs self-organize into large clusters, preferentially orient parallel to each other within a given cluster, and these clusters assume trans-membrane positions within each of the configurations). In the following section of the paper, we focus solely on the hairy nanotubes. The main reason for our interest in the self-assembly of hairy NTs and lipids is that, as we noted in the introduction, the hairs could be a key to regulating the trans-membrane traffic. And, importantly, while bare NTs can spontaneously insert into a lipid bilayer, such spontaneous insertion is not possible for the hairy NTs.[47] Hence, the self-assembly of hairy NTs and lipids could provide the only route to creating a number of hybrid NT−lipid structures that permit controlled transport through the membranes.

In the following studies, we systematically vary the number of hairy NTs from 0 to 18 (while fixing the number of amphiphilic beads at 5.6% of all the beads in our simulation box). We present results obtained from averaging over eight independent runs for each case and thus, generalize our findings on the self-assembly of the nanotubes and lipids in solution.

The aggregation of the species in these mixtures is a free-energy minimizing process (see Figure 4a), which involves reducing the number of unfavorable interactions, and proceeds by minimizing the number of interfaces. We demonstrate the interface minimization during the aggregation process for the various systems (the legend indicates the number of functionalized nanotubes in each system) by computing the time evolution of the solvent−lipid head interaction count per lipid molecule (see Figure 5a) and the solvent−lipid tail interaction count per lipid molecule (see Figure 5b). The insets in each graph highlight the interaction counts within the time frame of 10^4 to 4×10^4. Both the interaction counts fluctuate about steady-state values after the formation of a single aggregate. As could be anticipated, these steady-state values decrease with the increase in the fraction of the NTs (and hence, with the respective decrease in the fraction of the lipids in the system). Our studies indicate that the

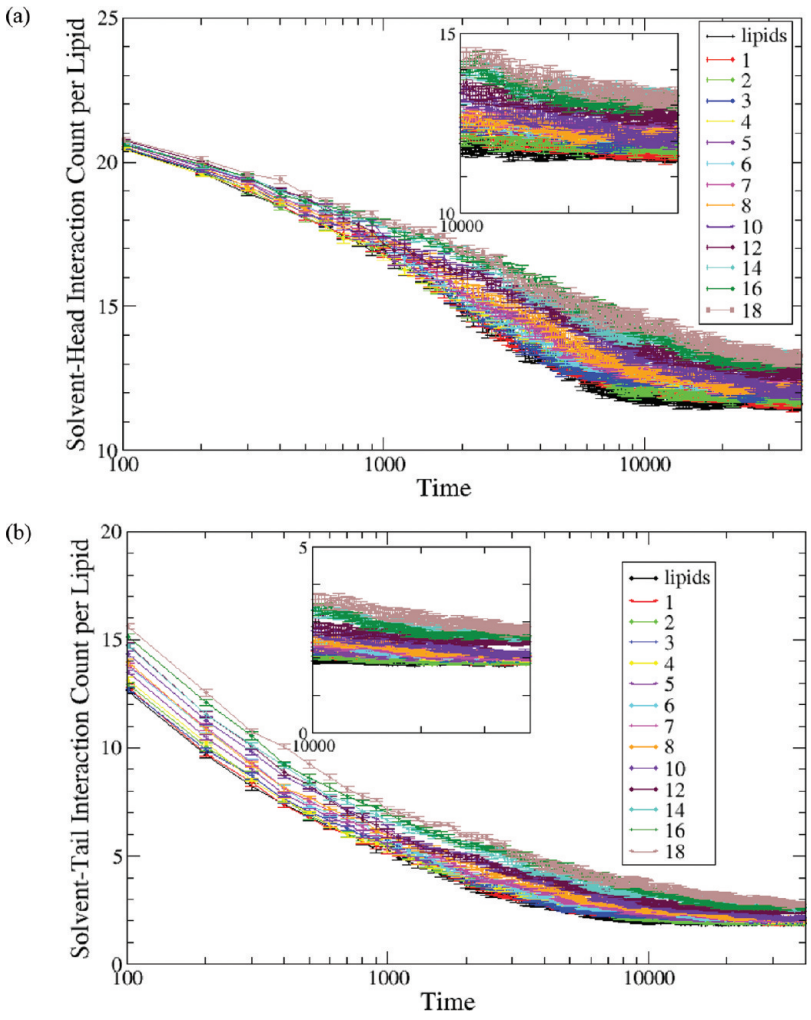

Figure 5. Time evolution of the (a) solvent-head interaction count per lipid and (b) solvent-tail interaction count per lipid, for pure lipids and mixtures of lipids and end-functionalized NTs. The legend shows the number of NTs in each system. The data set marked "lipids" indicates a pure lipid system. The insets in (a) and (b) show the data for the times 10^4 to 4×10^4. Here and below, the error bars are calculated based on eight independent simulation runs.

dynamics of the aggregation process is notably similar for all the cases considered (from the pure lipid system to systems with the number of NTs varying from 1 to 18).

To quantify the rate of aggregation, we calculate the number of clusters and the average cluster size during the course of the self-assembly process. Here, we define a cluster as a collection of nonsolvent beads (*i.e.*, lipid and NTs beads), which are within a cutoff interaction distance r_c from at least one of their neighbors. Therefore, a cluster i encompasses all nonsolvent beads that are interacting with at least one other member of the cluster i, and the total number of beads participating in a cluster i is denoted as n_c^i. At a specific time t, the total number of clusters for a given system is the maximum value of i, i_{max}, and the average cluster size n_c^{ave} is given by $n_c^{ave} = (\sum_{imax}^{i} n_c^i)/i_{max}$. We calculate the time evolution of the number of clusters (i_{max}) and the average cluster size (n_c^{ave}) for systems with different numbers of functionalized nanotubes and average over eight independent simulations.

Figure 6 shows the time evolution of the average cluster size (see Figure 6a) and the number of clusters (see Figure 6b) for systems with a varying number of nanotubes (indicated in the legend) but with the total concentration of lipids and nanotubes fixed at 5.6%. For the lipid/solvent system (no NTs), we find that the scaling exponent of the average cluster size with time is approximately 1, or $n_c^{ave} \propto t^{\alpha}$ where $\alpha \approx 1$. This result is in a good agreement with the prior simulation studies on the dynamics of self-assembly in lipid-solvent mixtures.[16] We emphasize that in the above studies, we define the cluster size by counting the number of beads in the cluster (similar to the definition of the cluster size in ref 16). Since the density in our system is approximately constant, the value of n_c^{ave} calculated above effectively gives the volume of the cluster (occupied by the nonsolvent molecules); hence, the linear size of the cluster scales as $R \approx (n_c^{ave})^{1/3} = t^{1/3}$ (assuming a spherical shape of the average cluster). Thus, the growth exponent we find in our studies is in

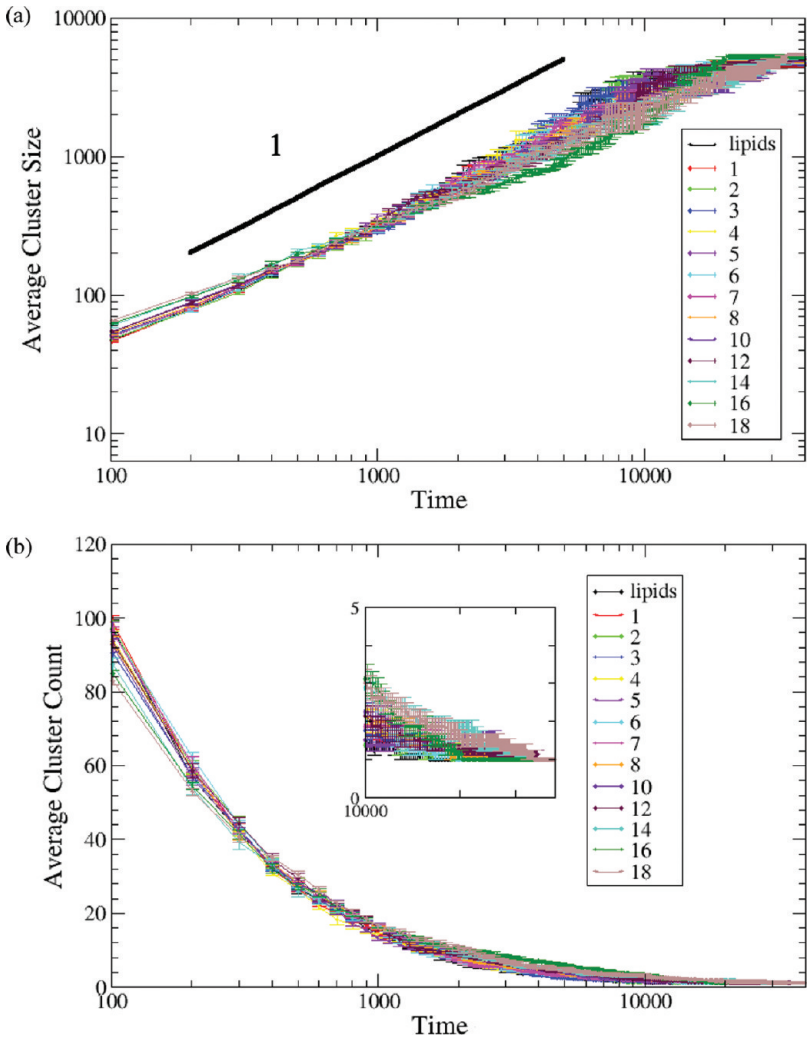

Figure 6. Time evolution of (a) the average cluster size and (b) the average cluster count for a pure lipid system and mixtures of lipids and end-functionalized NTs. The legend shows the number of NTs in each system. The line in panel a serves to indicate a growth exponent of 1. The growth exponents for the systems with different numbers of NTs are provided in Table 1. The inset in panel b shows the average cluster count for times 10^4 to 4×10^4.

agreement with the Lifshits−Slyozov growth exponent describing the coarsening dynamics during the phase separation of binary mixtures at early times.[79] The same growth exponent ($R \approx t^{1/3}$) was reported in an experimental study on the self-assembly of unilamellar vesicles.[22]

As compared to the pure lipid/solvent system, our results indicate a slight decrease in the growth exponent with an increase in the fraction of end-functionalized nanotubes; namely, α decreases to approximately $\alpha \approx 0.8$ for the systems with larger numbers of NTs, where stable bicelles are formed (see Table 1). In agreement with these calculations, we also find that the average cluster count, i_{max}, scales with time as $i_{max} \propto t^{\beta}$, where $\beta \approx -1$ for systems with smaller numbers of NTs (when a hybrid vesicle is formed), and decreases to approximately $\beta \approx -0.8$ with larger numbers of NTs (when a stable bicelle is formed) (see Table 1). Calculations of the exponents provided in Table 1 (for both average cluster size and the cluster count) span a time interval from the beginning of the aggregation process to the formation of a single aggregate. Our results on the cluster growth rate, together with the results on the interface minimization, indicate that the dynamics of the system remains remarkably similar for all the cases considered here: from the pure lipid system to the systems with the number of NTs varying from 1 to 18.

In the above examples (Figures 2 and 3), we illustrated two distinctly different types of NTs organization within the late-time, nanostructured aggregates. It is likely that a depletion attraction[34,35,39,80−84] between the NTs is the leading cause for the clustering we observe in our studies. In the cases considered here, the conformational entropy of the lipid tails is reduced when these moieties lie near the nanotube shaft. The drive to maximize the entropy of the system induces an attractive force that effectively pushes the nanotubes together. This phenomenon has been observed in earlier studies of nanoparticles or model proteins interacting with lipid membranes.[34,35,39−41,43]

To gain further insight into the NT interaction and self-organization, we systematically vary the number of NTs from 1 to 18. In particular, we calculate the number of nanotube clusters during the course of the entire simulation in each of the cases. (Recall that the NT cluster is defined as a number of nanotubes that are effectively "in contact"). Figure 7 shows the time evolution of the average number of NT clusters, $\langle k \rangle$, for the cases of hybrid vesicle formation (7 and 10 NTs, marked by the black and red lines, respectively), and for the cases of nanostructured bicelles formation (cases for 12, 14, 16, and 18 NTs). In each of the curves, we average the number of NT clusters over eight independent runs.

TABLE 1. Growth Exponents for Cluster Size and Count Measurements

number of NTs	exponent calculated from cluster size data	exponent calculated from cluster count data
0	1.05	−0.97
1	0.97	−0.96
2	0.98	−0.90
3	1.09	−1.01
4	0.88	−0.90
5	0.89	−0.87
6	0.91	−0.95
7	0.97	−0.94
8	0.91	−0.86
10	0.94	−0.87
12	0.88	−0.85
14	0.81	−0.76
16	0.81	−0.76
18	0.81	−0.76

As seen in Figure 4c, the total number of NT clusters decreases in a stepwise manner for a given run; averaged over eight runs, this decrease is relatively smooth (see Figure 7). At early times, we observe a faster decrease in $\langle k \rangle$ (a faster NT clustering rate) for the larger number of NTs; this can be attributed to the shorter average distances between the NTs.

At later times, the number of NT clusters saturates to steady-state values in all the cases; for clarity, the late time dynamics is shown in the inset to Figure 7. We note that significantly longer times are needed to reach the steady-state distribution of NT clusters than to form a single cluster encompassing all the amphiphilic species (see Figure 6b). Namely, as we showed above, a single aggregate encompassing all the lipids and NTs is already formed in the majority of the cases at times in the range of 10^4 to 2×10^4; during the same time frame, the total number of interfaces in the majority of cases has also reached its minimal values (see Figure 5). The restructuring of the NTs clusters, however, continues well beyond this time frame; as can be seen from the inset in Figure 7, the saturation values of the NT clusters, $\langle k \rangle$, are reached only by the time interval of 4×10^4 to 6×10^4 for all the cases considered here. This clearly indicates that NTs (or clusters of NTs) continue to diffuse within the single aggregate and form larger clusters until the steady-state NT distribution is reached. Additional calculations showed that in all the cases considered here, the late-time restructuring of the NT clusters does not change the NT−NT interaction count and the total average energy (during the late-time NT clustering, both values change within the range of fluctuations, as we illustrated for two representative cases in Figure 4d).

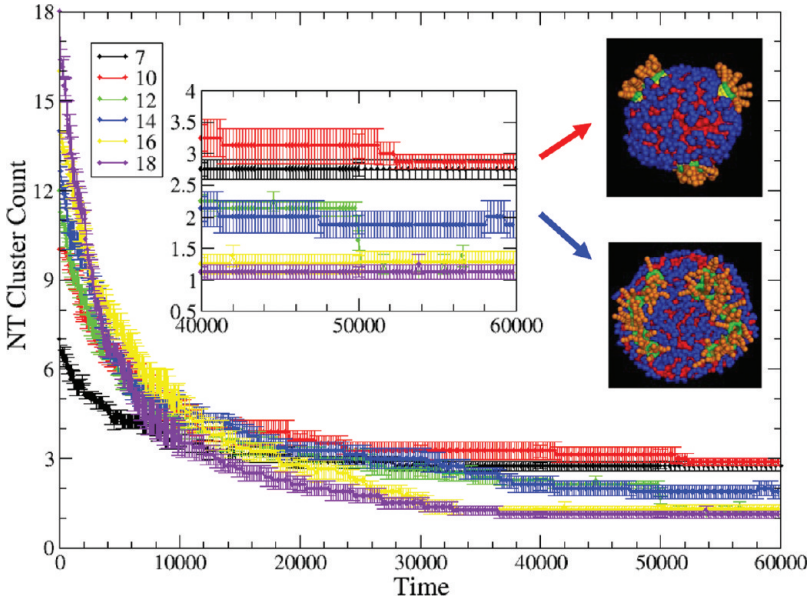

Figure 7. Time evolution of the number of NT clusters for systems with different number of NTs (indicated in the legend). The inset highlights the results for late times (4×10^4 to 6×10^4). The inset on the upper right corner shows the hybrid NT−lipid vesicle for a system with 10 NTs. The inset on the lower right corner illustrates a stable bicelle in a system with 14 NTs .

TABLE 2. Average Number and Distribution of NT Clusters

		number of cases (out of 8) with k NTs clusters				
number of NTs	average number $\langle k \rangle$ of NT clusters	$k = 5$	$k = 4$	$k = 3$	$k = 2$	$k = 1$
3	2.375	0	0	5	1	2
4	2.75	0	1	4	1	0
5	3.125	1	1	4	2	0
6	2.875	0	1	5	2	0
7	2.75	0	0	6	2	0
8	3.25	0	2	6	0	0
10	3.25	1	1	5	1	0

Our results show that for the systems with seven and ten functionalized nanotubes, which generate a stable vesicle, the late-time nanotube cluster count is 2.9 $\pm$ 0.1 (see Figure 7). Namely, in the majority of cases the transmembrane NTs form three distinct clusters (similar to the distribution shown in Figure 2e,f). For example, for the system with 10 NTs, at the latest instant of time considered in our studies ($t = 6 \times 10^4$), in seven out of eight independent simulation runs, we observe the formation of three NT clusters; it is only in one case that two large NT clusters (located at the poles of the vesicle) are formed.

For NT numbers varying from three to 10, we also find that the formation of three NT clusters is robust process that occurs in the majority of the cases (as long as the late time dynamics results in the formation of a hybrid vesicle). Table 2 provides more detailed information on the number of NT clusters within these vesicles (calculated at time $t = 4 \times 10^4$) and shows that the average number of clusters is close to three in all of the cases.

The NTs clustering is significantly different for the larger fractions of NTs where components self-assemble into bicelles (see curves corresponding to NT numbers of 12 and higher in Figure 7). For these systems, in the majority of cases we observe the formation of one or two large clusters. These clusters tend to be located close to the edges of the bicelles (see inset for NTs = 14 in Figure 7 and Figure 3c–e). We note that the bending rigidity of the hybrid bicelles increases with the addition of a higher fraction of NTs; thus, while the structures we observe with 12 and 14 NTs are relatively "floppy" (especially for the case of 12 NTs), the bicelles with 16 and 18 NTs remain relatively flat.

CONCLUSIONS

We undertook the first computational studies of the self-assembly of mixtures of hairy nanotubes and lipids in an aqueous solution and thereby demonstrated that these components can spontaneously organize into stable vesicles or bicelles. For relatively low fractions of NTs, the self-assembly process provides a route for integrating nanotubes with hairs at both ends into the bilayer of a vesicle, and thus, creating a cellular object with biomimetic membrane-spanning channels. We showed that such nanostructured, hybrid vesicles form through a transient bicelle-to-vesicle transition, similar to vesicle formation in the pure lipid/solvent systems. Notably, we found that the nanotubes self-organize into a tripod-like structure (shown in Figure 1d and Figure 2) within these vesicles.

For higher fractions of NTs, the system associates into a hybrid bicelle structure, with the NTs clustering into a ring-like arrangement, which lies close to the edges of the bicelle (shown in Figure 1e and Figure 3). Our simulations provide the first evidence that an increase in the fraction of the NTs prevents the late time bicelle-to-vesicle transition and hence, yields a stable, hybrid bicelle.

In addition to characterizing the equilibrium morphology of the vesicles and bicelles, we systematically varied the fraction of NTs to determine the growth rate of clusters formed by amphiphilic species during the assembly process. Furthermore, we determined the temporal evolution of the interactions between the nanotubes during the self-assembly and the subsequent rearrangements of the nanotube clusters within the self-assembled structures.

Our results indicate that the self-assembly of hairy nanotubes and lipids in solution provides a new route for the spontaneous creation of nanotube clusters with distinct morphologies. The NT clusters can be stabilized by chemically cross-linking the tethered hairs and can be extracted from the lipid assemblies to be used in other applications. In this manner, the vesicles and bicelles form microreactors of forging nanotube clusters with tunable morphologies.

The hydrophilic hairs, which extend into the external solution and the interior of the vesicle, also provide a means of reversibly opening or closing the transmembrane nanotube channels and thus, regulating the traffic through the vesicle's membrane. Namely, by varying temperature or pH, the hairs can be made to extend or collapse and thus, open or close the nanotube pores. The hybrid vesicles with controllable pores can constitute a fundamental building block in the formation of synthetic cells that exhibit biomimetic functionality. The responsiveness of the hairs also permits the regulated release of encapsulated species and thus, the hybrid assemblies could be useful in controlled release applications.

METHODOLOGY

Similar to MD simulations, DPD captures the temporal evolution of a many-body system through the numerical integration of Newton's equation of motion, $m(d\mathbf{v}_i/dt) = \mathbf{f}_i$, where the mass m of a bead of any species is set to 1. Unlike MD simulations, DPD involves the use of soft, repulsive interactions and a

momentum-conserving thermostat.[59] The force acting on a bead consists of three parts, each of which is pairwise additive: $\mathbf{f}_i(t) = \sum(\mathbf{F}_{ij}^{C} + \mathbf{F}_{ij}^{D} + \mathbf{F}_{ij}^{R})$, where the sum runs over all beads j within a certain cutoff radius r_c. The conservative force is a soft, repulsive force given by $\mathbf{F}_{ij}^{C} = a_{ij}(1 - r_{ij})\hat{\mathbf{r}}_{ij}$, where a_{ij} is the maximum repulsion between beads i and j, $r_{ij} = |\mathbf{r}_i - \mathbf{r}_j|/r_c$, and $\hat{\mathbf{r}}_{ij} = \mathbf{r}_{ij}/|\mathbf{r}_{ij}|$. The drag force is $\mathbf{F}_{ij}^{D} = -\gamma\omega_D(r_{ij})(\hat{\mathbf{r}}_{ij}\cdot\mathbf{v}_{ij})\hat{\mathbf{r}}_{ij}$, where γ is a simulation parameter related to viscosity, ω_D is a weight function that goes to zero at r_c, and $\mathbf{v}_{ij} = \mathbf{v}_i - \mathbf{v}_j$. The random force is $\mathbf{F}_{ij}^{R} = \sigma\omega_R(r_{ij})\xi_{ij}\hat{\mathbf{r}}_{ij}$, where ξ_{ij} is a zero-mean Gaussian random variable of unit variance and $\sigma^2 = 2k_BT\gamma$. Finally, we use $\omega_D(r_{ij}) = \omega_R(r_{ij})^2 = (1 - r_{ij})^2$ for $r_{ij} < r_c$.[59] Because all three of these forces conserve momentum locally, hydrodynamic behavior emerges even in systems containing only a few hundred particles.[59] The equations of motion are integrated in time with a modified velocity-Verlet algorithm.[85]

We take r_c as the characteristic length scale and k_BT as the characteristic energy scale in our simulations. A characteristic time scale is then defined as $\tau = (mr_c^2/k_BT)^{1/2}$. The remaining simulation parameters are $\sigma = 3$ and $\Delta t = 0.02\tau$ with a total bead number density of $\rho = 3$ and a dimensionless value of $r_c = 1$.[73]

As shown in Figure 1b, our system contains short-chain lipids. The bonds between beads in the chain are represented by the harmonic spring potential $E_{bond} = K_{bond}((r - b)/r_c)^2$, where K_{bond} is the bond constant and b is the equilibrium bond length. We use $K_{bond} = 64$ and $b = 0.5$.[73]

The hydrophobic shaft of the nanotube is formed from a stack of seven concentric rings. Each ring has a radius of 1.5 and contains 13 beads; the spacing between the centers of neighboring beads on a given ring is 0.5, and the distance between the center of a bead and its nearest neighbor on an adjacent layer is also 0.5. (All distances here and below are given in units of r_c, which is the characteristic interaction range and, as noted above, is set to $r_c = 1$ in dimensionless units.) There is perfect hydrophobic matching between the nanotube and the bilayer,[47] namely, the length of the nanotube's hydrophobic shaft is chosen to be equal to the width of the hydrophobic part of the lipid membrane. The hydrophilic domain in the nanotube is formed from a single ring of beads (drawn in green in Figure 1a) that are located on both ends of the shaft. The nanotubes encompass end-tethered chains, which emanate from both the hydrophilic end rings and are attached at equally spaced intervals. The length of the tethers is fixed at four hydrophilic beads. Within the nanotube, there is no interaction between the hydrophilic ring (green beads in Figure 1a) and the hydrophobic shaft; the hydrophilic tethers do, however, interact with each other and the hydrophobic shaft. The bond potential parameters for the hydrophilic tethers are the same as those for the lipid tails. Additionally, we include a three-body stiffness potential along the tethers of the form $E_{angle} = K_{angle}(1 + \cos\theta)$ where θ is the angle formed by three adjacent tether beads,[62,73] and we set the coefficient to $K_{angle} = 20$.

The amphiphilic nature of the lipids is captured by specifying the repulsive interactions between the components. Our choices for the interaction parameters between the components, a_{ij}, are based on the available data, as explained below. For any two beads of the same type, we take the repulsion parameter to be $a_{ii} = 25$ (measured in units of k_BT). This a_{ii} is equal to the value calculated by Groot and Warren[48] based on the compressibility of water for the chosen dimensionless density of $\rho = 3$. The excess repulsion between the hydrophobic–hydrophilic beads can be calculated based on the Flory–Huggins interaction parameters, χ, as $a_{ij} = a_{ii} + 3.496\chi$.[59] Note that the latter expression is written for the fixed density $\rho = 3$ and is valid for relatively high values of χ, that is, sufficiently far from the critical point.[59] Here, we chose the value of the interaction parameter between the different hydrophobic–hydrophilic moieties as $a_{ij} = 100$. Given that S stands for solvent, H stands for a lipid head bead, and T stands for a lipid tail bead, we specifically set $a_{SS} = 25$, $a_{HS} = 25$, $a_{HT} = 100$, and $a_{ST} = 100$. These values were used in a number of previous DPD simulations of lipid bilayers[73,74] and as previously observed,[62,73] we find that lipids spontaneously self-assemble into bilayers for these interaction parameters.

To capture the amphiphilic nature of the nanotube, we specify an additional set of interactions parameters to account for the unfavorable interactions between the nanotube's hydrophobic shaft and the solvent, and between this shaft and the hydrophilic tethered chains. The hydrophilic hairs could be PEG (polyethylene glycol, $C_{2n+2}H_{4n+6}O_{n+2}$, see ref 54) or AZT (3′-azido-3′-deoxythymidine, see ref 53). In the following notation, s stands for the hydrophobic shaft beads, e stands for the band of hydrophilic beads at both ends of the hydrophobic shaft, and t stands for beads making up the hydrophilic tethered chains. Given this notation, we set $a_{Tt} = 100$, $a_{Ts} = 25$, $a_{Te} = 100$, $a_{Ht} = 25$, $a_{Hs} = 100$, $a_{He} = 25$, $a_{St} = 25$, $a_{Ss} = 100$, $a_{Se} = 25$, $a_{tt} = 25$, $a_{ts} = 100$, and $a_{te} = 100$. Note that we chose the values of the parameters describing the interactions between all the hydrophobic and hydrophilic moieties to be $a_{ij} = 100$. The same values were previously used to describe the respective interactions between the hydrophobic and hydrophilic beads of hard Janus particles and a lipid bilayer[74] and end-functionalized amphiphilic nanotubes and lipid bilayer.[47]

The simulation parameters can be related to physical length and time scales by examining the properties of a tensionless membrane.[73] The lipids in our investigations represent DPPC (dipalmitoylphosphatidycholine, $C_{40}H_{80}NO_8P$). Typical experimental measurements of DPPC membranes[73] in a tensionless state yield an equilibrium area per lipid of approximately 0.6 nm^2. This value can be used to establish a dimensional length scale in the DPD simulations and gives $r_c = 0.67$ nm.[73] The DPD time scale τ can be estimated from the in-plane diffusion constant of lipids, which, for a flat DPPC membrane, has been measured[73] as $D = 5$ μm^2/s. By matching the latter value to the diffusion constant in a simulation, we obtain $\tau = 7.2$ ns and, for a single time step, $\Delta t = 0.02\tau = 0.14$ ns.[73]

Acknowledgment. The authors gratefully acknowledge support from the NSF. Portions of the research were conducted using high performance computational resources at the Louisiana Optical Network Initiative (http://www.loni.org), the National Institute for Computational Sciences (http://www.nics.tennessee.edu) through the Teragrid (TG-MCB090174), and the Center of Molecular and Materials Simulation (http://core.sam.pitt.edu) at the University of Pittsburgh.

Supporting Information Available: One movie on the dynamics of the self-assembly of a hybrid vesicle; one movie on the dynamics of the edge fusion of a transient bicelle to form a vesicle; one movie on the dynamics of the self-assembly of a hybrid bicelle; one figure of the snapshots of a vesicle and a bicelle obtained from the self-assembly of amphiphilic lipid molecules and bare nanotubes; one figure of the time evolution of the average pair energy of hybrid systems with 10 and 14 hairy NTs; one figure of the time evolution of the average bond energy of hybrid systems with 10 and 14 hairy NTs; one figure of the time evolution of the average angle energy of hybrid systems with 10 and 14 hairy NTs; one figure of the time evolution of the average total energy of hybrid systems with 10 hairy NTs; one figure of the state diagram of the morphology of the lipid–NT hybrid systems.This material is available free of charge *via* the Internet at http://pubs.acs.org.

REFERENCES AND NOTES

1. Israels, R.; Gersappe, D.; Fasolka, M.; Roberts, V. A.; Balazs, A. C. pH-Controlled Gating in Polymer Brushes. *Macromolecules* **1994**, *27*, 6679–6682.
2. Manna, L.; Scher, E. C.; Alivisatos, A. P. Synthesis of Processable Rod-, Arrow-, Teardrop-, and Tetrapod-Shaped CdSe Nanocrystals. *J. Am. Chem. Soc.* **2000**, *122*, 12700–12706.
3. Dong, L.; Gushtyuk, T.; Jiao, J. Synthesis, Characterization, and Growth Mechanism of Self-Assembled Dendritic CdS Nanorods. *J. Phys. Chem. B* **2004**, *108*, 1617–1620.
4. Yamamoto, S.; Maruyama, Y.; Hyodo, S. Dissipative Particle Dynamics Study of Spontaneous Vesicle Formation of Amphiphilic Molecules. *J. Chem. Phys.* **2002**, *116*, 5842–5849.
5. Antonietti, M.; Forster, S. Vesicles and Liposomes: A Self-Assembly Principle Beyond Lipids. *Adv. Mater.* **2003**, *15*, 1323–1333.

6. Shinoda, W.; De Vane, R.; Klein, M. L. Zwitterionic Lipid Assemblies: Molecular Dynamics Studies of Monolayers, Bilayers and Vesicles Using a New Coarse Grain Force Field. *J. Phys. Chem. B* **2010**, *114*, 6836–6849.
7. Noguchi, H.; Takasu, M. Self-Assembly of Amphiphiles into Vesicles: A Brownian Dynamics Simulation. *Phys. Rev. E* **2001**, *64*, 041913.
8. Huang, J.; Wang, Y.; Qian, C. Simulation Study on the Formation of Vesicle and Influence of Solvent. *J. Chem. Phys.* **2009**, *131*, 234902.
9. Marrink, S. J.; Mark, A. E. Molecular Dynamics Simulation of the Formation, Structure and Dynamics of Small Phospholipid Vesicles. *J. Am. Chem. Soc.* **2003**, *125*, 15233–15242.
10. Marrink, S. J.; Mark, A. E. Simulations of the Spontaneous Aggregation of Phospholipids into Bilayers. *J. Am. Chem. Soc.* **2003**, *125*, 15233–15242.
11. Marrink, S. J.; Tieleman, D. P.; Mark, A. E. Molecular Dynamics Simulations of the Kinetics Spontaneous Micelle Formation. *J. Am. Chem. Soc.* **2003**, *125*, 15233–15242.
12. Wang, Z.; He, X. Dynamics of Vesicle Formation from Liquid Droplets: Mechanism and Controllability. *J. Chem. Phys.* **2009**, *130*, 094905.
13. Fujiwara, S.; Itoh, T.; Hashimoto, M.; Horiuchi, R. Molecular Dynamics Simulation of Amphiphilic Molecules in Solution: Micelle Formation and Dynamics Coexistence. *J. Chem. Phys.* **2009**, *130*, 144901.
14. Leng, J.; Egelhaaf, S. U.; Cates, M. E. Kinetic Pathway of Spontaneous Vesicle Formation. *Europhys. Lett.* **2002**, *59*, 311–317.
15. Leng, J.; Egelhaaf, S. U.; Cates, M. E. Kinetics of Micelle-to-Vesicle Transition: Aqueous Lecithin-Bile Salt Mixtures. *Biophys. J.* **2003**, *85*, 1624–1646.
16. Noguchi, H.; Gompper, G. Dynamics of Vesicle Self-Assembly and Dissolution. *J. Chem. Phys.* **2006**, *125*, 164908.
17. Goetz, R.; Gompper, G.; Lipowsky, R. Mobility and Elasticity of Self-Assembled Membranes. *Phys. Rev. Lett.* **1999**, *82*, 221–224.
18. Goetz, R.; Lipowsky, R. Computer Simulations of Bilayer Membranes: Self-Assembly and Interfacial Tension. *J. Chem. Phys.* **1998**, *108*, 7397–7409.
19. Cooke, I. R.; Deserno, M. Solvent-free Model for Self-Assembling Fluid Bilayer Membranes: Stabilization of the Fluid Phase Based on Broad Attractive Tail Potentials. *J. Chem. Phys.* **2005**, *123*, 224710.
20. Cooke, I. R.; Deserno, M. Coupling Between Lipid Shape and Membrane Curvature. *Biophys. J.* **2006**, *91*, 487–495.
21. Wang, Z.-J.; Deserno, M. A Systematically Coarse-Grained Solvent-free Model for Quantitative Phospholipid Bilayer Simulations. *J. Phys. Chem. B* **2010**, *114*, 11207–11220.
22. Weiss, T. M.; Narayanan, T.; Wolf, C.; Gradzielski, M.; Panine, P.; Finet, S.; Helsby, W. I. Dynamics of the Self-Assembly of Unilamellar Vesicles. *Phys. Rev. Lett.* **2005**, *94*, 038303.
23. Weiss, T. M.; Narayanan, T.; Gradzielski, M. Dynamics of Spontaneous Vesicle Formation in Fluorocarbon and Hydrocarbon Surfactant Mixtures. *Langmuir* **2008**, *24*, 3759–3766.
24. Shioi, A.; Hatton, T. A. Model for Formation and Growth of Vesicles in Mixed Anionic/Cationic (SOS/CTAB) Surfactant Systems. *Langmuir* **2002**, *18*, 7341–7348.
25. Yamamoto, S.; Hyodo, S. Budding and Fission Dynamics of Two-Component Vesicles. *J. Chem. Phys.* **2003**, *118*, 7937–7943.
26. Laradji, M.; Kumar, P. B. S. Dynamics of Domain Growth in Self-Assembled Fluid Vesicles. *Phys. Rev. Lett.* **2004**, *93*, 198105.
27. Laradji, M.; Kumar, P. B. S. Anomalously Slow Domain Growth in Fluid Membranes with Asymmetric Transbilayer Lipid Distribution. *Phys. Rev. E* 2006, *73*, 040910(R).
28. Laradji, M.; Kumar, P. B. S. Domain Growth, Budding and Fission in Phase-Separating Self-Assembled Fluid Bilayers. *J. Chem. Phys.* **2005**, *123*, 224902.
29. Zheng, C.; Liu, P.; Li, J.; Zhang, Y.-W. Phase Diagrams for Multicomponent Membrane Vesicles: A Coarse-Grained Modeling Study. *Langmuir* **2010**, *26*, 12659–12666.
30. Venturoli, M.; Smit, B.; Sperotto, M. M. Simulation Studies of Protein-Induced Bilayer Deformations, and Lipid-Induced Protein Tilting, on a Mesoscopic Model for Lipid Bilayers with Embedded Proteins. *Biophys. J.* **2005**, *88*, 1778–1798.
31. Yue, T.; Li, S.; Zhang, X.; Wang, W. The Relationship Between Membrane Curvature Generation and Clustering of Anchored Proteins: A Computer Simulation Study. *Soft Matter* **2010**, *6*, 6109–6118.
32. Illya, G.; Deserno, M. Coarse-Grained Simulation Studies of Peptide-Induced Pore Formation. *Biophys. J.* **2008**, *95*, 4163–4173.
33. Li, S.; Zhang, X.; Wang, W. Cluster Formation of Anchored Proteins Induced by Membrane-Mediated Interaction. *Biophys. J.* **2010**, *98*, 2554–2563.
34. Sintes, T.; Baumgartner, A. Protein Mediated Attraction in Membranes Induced by Lipid Fluctuations. *Biophys. J.* **1997**, *73*, 2251–2259.
35. de Meyer, F.J.-M.; Venturoli, M.; Smit, B. Molecular Simulation of Lipid-Mediated Protein−Protein Interactions. *Biophys. J.* **2008**, *95*, 1851–1865.
36. de Meyer, F.J.-M.; Rodgers, J. M.; Willems, T. F.; Smit, B. Molecular Simulation of the Effect of Cholesterol on Lipid-Mediated Protein−Protein Interactions. *Biophys. J.* **2010**, *99*, 3629–3638.
37. Yiannourakou, M.; Marsella, L.; de Meyer, F.; Smit, B. Towards an Understanding of Membrane-Mediated Protein−Protein Interactions. *Faraday Discuss.* **2010**, *144*, 359–367.
38. Philips, R.; Ursell, T.; Wiggins, P.; Sens, P. Emerging Roles for Lipids in Shaping Membrane-Protein Function. *Nature* **2009**, *469*, 379–385.
39. Gil, T.; Ipsen, J. H.; Mouritsen, O. G.; Sabra, M. C.; Sperotto, M. M.; Zuckermann, M. J. Theoretical Analysis of Protein Organization in Lipid Membranes. *Biochim. Biophys. Acta* **1998**, *1376*, 245–266.
40. Weikl, T. R. Fluctuation-Induced Aggregation of Rigid Membrane Inclusions. *Europhys. Lett.* **2001**, *54*, 547–553.
41. Dan, N.; Pincus, P.; Safran, S. A. Membrane-Induced Interactions between Inclusions. *Langmuir* **1993**, *9*, 2768–2771.
42. Netz, R. R.; Pincus, P. Inhomogeneous Fluid Membranes: Segregation, Ordering and Effective Rigidity. *Phys. Rev. E* **1995**, *52*, 4114–4128.
43. Aranda-Espinoza, H.; Berman, A.; Dan, N.; Pincus, P.; Safran, S. Interaction Between Inclusions Embedded in Membranes. *Biophys. J.* **1996**, *71*, 648–656.
44. West, B.; Brown, F. L. H.; Schmid, F. Membrane−Protein Interactions in a Generic Coarse-Grained Model for Lipid Bilayers. *Biophys. J.* **2009**, *96*, 101–115.
45. Lopez, C. F.; Nielsen, S. O.; Moore, P. B.; Klein, M. L. Understanding Nature's Design for a Nanosyringe. *Proc. Natl. Acad. Sci., U.S.A.* **2004**, *101*, 4431–4434.
46. Lopez, C. F.; Nielsen, S. O.; Ensing, B.; Moore, P. B.; Klein, M. L. Structure and Dynamics of Model Pore Insertion into a Membrane. *Biophys. J.* **2005**, *88*, 3083–3094.
47. Dutt, M.; Kuksenok, O.; Little, S. R.; Balazs, A. C. Forming Transmembrane Channels Using End-Functionalized Nanotubes. *Nanoscale* **2011**, *3*, 240–250.
48. Gu, Z.; Peng, H.; Hauge, R. H.; Smalley, R. E.; Margrave, J. L. Cutting Single-Wall Carbon Nanotubes through Fluorination. *Nano Lett.* **2002**, *2*, 1009–1013.
49. Wang, S.; Liang, Z.; Wang, B.; Zhang, C.; Rahman, Z. Precise Cutting of Single-Walled Carbon Nanotubes. *Nanotechnology* **2007**, *18*, 055301.
50. Javey, A.; Qi, P.; Wang, Q.; Dai, H. 10- to 50-nm-long Quasi-Ballistic Carbon Nanotubes Devices Obtained Without Complex Lithography. *Proc. Natl. Acad. Sci. U.S.A.* **2004**, *101*, 13408–13410.
51. Sun, X.; Zaric, S.; Daranciang, D.; Welsher, K.; Lu, Y.; Li, X.; Dai, H. Optical Properties of Ultrashort Semiconducting Single-Walled Carbon Nanotube Capsules Down to Sub-10nm. *J. Am. Chem. Soc.* **2008**, *130*, 6551–6555.
52. Balasubramanian, K.; Burghard, M. Chemically Functionalized Carbon Nanotubes. *Small* **2005**, *1*, 180–192.

53. Lee, K. M.; Li, L.; Dai, L. Asymmetric End-Functionalization of Multiwalled Carbon Nanotubes. *J. Am. Chem. Soc.* **2005**, *127*, 4122–4123.
54. Stephenson, J. J.; Hudson, J. L.; Leonard, A. D.; Price, K.; Tour, J. M. Repetitive Functionalization of Water-Soluble Single-Walled Carbon Nanotubes. Addition of Acid-Sensitive Addends. *Chem. Mater.* **2007**, *19*, 3491–3498.
55. Chattopadhyay, J.; Cortez, F.d.J.; Chakraborty, S.; Slater, N. K. H.; Billups, W. E. Synthesis of Water-Soluble PEGylated Single-Walled Carbon Nanotubes. *Chem. Mater.* **2006**, *18*, 5864–5868.
56. Liu, Z.; Shen, Z.; Zhu, T.; Hou, S.; Ying, L. Organizing Single-Walled Carbon Nanotubes on Gold Using a Wet Chemical Self-Assembling Technique. *Langmuir* **2000**, *16*, 3569–3573.
57. Chen, Z.; Kobashi, K.; Rauwald, U.; Booker, R.; Fan, H.; Hwang, W.-F.; Tour, J. M. Soluble Ultrashort Single-Walled Carbon Nanotubes. *J. Am. Chem. Soc.* **2006**, *128*, 10568–10571.
58. Ashcroft, J. M.; Hartman, K. B.; Mackeyav, Y.; Hofman, C.; Pheasant, C.; Alemany, L. B.; Wilson, L. J. Functionalization of Individual Ultrashort Single-Walled Carbon Nanotubes. *Nanotechnology* **2006**, *17*, 5033–5037.
59. Groot, R. D.; Warren, P. B. Dissipative Particle Dynamics: Bridging the Gap Between Atomistic and Mesoscopic Simulation. *J. Chem. Phys.* **1997**, *107*, 4423–4435.
60. Illya, G.; Lipowsky, R.; Shillcock, J. C. Effect of Chain Length and Asymmetry on Material Properties of Bilayer Membranes. *J. Chem. Phys.* **2005**, *122*, 244901.
61. Groot, R. D.; Rabone, K. L. Mesoscopic Simulation of Cell Membrane Damage, Morphology Change and Rupture by Nonionic Surfactants. *Biophys. J.* **2001**, *81*, 725–736.
62. Shillcock, J. C.; Lipowsky, R. Equilibrium Structure and Lateral Stress Distribution of Amphiphilic Bilayers From Dissipative Particle Dynamics Simulations. *J. Chem. Phys.* **2002**, *117*, 5048–5061.
63. Kranenburg, M.; Venturoli, M.; Smit, B. Molecular Simulations of Mesoscopic Bilayer Phases. *Phys. Rev. E* **2003**, *67*, 060901.
64. Rekvig, L.; Kranenburg, M.; Vreede, J.; Hafskjold, B.; Smit, B. Investigation of Surfactant Efficiency Using Dissipative Particle Dynamics. *Langmuir* **2003**, *19*, 8195–8205.
65. When calculating the fraction of the amphiphilic species (NTs and lipids), we count all the lipid beads; however, we count only the NT beads in the rigid shaft (hydrophobic beads shown in yellow and hydrophilic caps shown in green in Figure 1b) and do not include the hydrophilic tethers. Hence, to add a given number of NTs to a simulation box of fixed size, we remove the number of lipids corresponding to the number of beads in the NTs (excluding the tethers), and remove the solvent beads to add the hydrophilic tethers. In this manner, the number density of the hydrophobic species in this system remains approximately constant (~4% of the hydrophobic beads in the simulation box). While the exact number of hydrophobic beads increases somewhat at a higher number of NTs, this increase is very small. For example, in the reference case involving only lipids and no NTs, 3.73% of the beads are hydrophobic, while in the case of 10 NTs, 3.89% of the beads are hydrophobic.
66. Wu, S.; Guo, H. Dissipative Particle Dynamics Simulation Study of Bilayer−Vesicle Transition. *Sci. Chin. Ser. B, Chem.* **2008**, *51*, 743–750.
67. Wu, S.; Lu, T.; Guo, H. Dissipative Particle Dynamics Simulation Study of Lipid Membrane. *Front. Chem. Chin.* **2010**, *5*, 288–298.
68. Fromherz, P. Lipid-Vesicle Structure: Size Control by Edge-Active Agents. *Chem. Phys. Lett.* **1983**, *94*, 259–266.
69. Fromherz, P.; Rocker, C.; Ruppel, D. From Discoid Micelles to Spherical Vesicles. The Concept of Edge Activity. *Faraday Discuss. Chem. Soc.* **1986**, *81*, 39–48.
70. Markvoort, A. J.; Pieterse, K.; Steijaert, M. N.; Spijker, P.; Hilbers, P. A. J. The Bilayer−Vesicle Transition Is Entropy Driven. *J. Chem. Phys. B* **2005**, *109*, 22649–22654.
71. Markvoort *et al.* showed[70] that in their system, the potential energy actually increased during the bicelle-to-vesicle transition and hence, they argued that this transition was entropically driven.
72. Wu, S.; Guo, H. Simulation Study of Protein-Mediated Vesicle Fusion. *J. Phys. Chem. B Lett.* **2009**, *113*, 589–591.
73. Smith, K. A.; Jasnow, D.; Balazs, A. C. Designing Synthetic Vesicles that Engulf Nanoscopic Particles. *J. Chem. Phys.* **2007**, *127*, 084703.
74. Alexeev, A.; Upsal, W. E.; Balazs, A. C. Harnessing Janus Nanoparticles to Create Controllable Pores in Membranes. *ACS Nano* **2008**, *2*, 1117–1122.
75. The bending rigidity of the membrane also depends on the length of the lipid tails.[76] Bilayers formed from lipids with a shorter tail will have a lower rigidity than those formed from lipids with a longer tail,[76] which would likely increase the fraction of NTs required to cause the vesicle-to-bicelle transition (assuming a perfect hydrophobic match of the NTs and membrane).
76. Rawicz, W.; Olbrich, K. C.; McIntosh, T.; Needham, D.; Evans, E. Effects of Chain Length and Unsaturation on Elasticity of Lipid Bilayers. *Biophys. J.* **2000**, *79*, 328–339.
77. Horsch, M. A.; Zhang, Z.; Glotzer, S. C. Self-Assembly of Polymer-Tethered Nanorods. *Phys. Rev. Lett.* **2005**, *95*, 056105.
78. Horsch, M. A.; Zhang, Z.; Glotzer, S. C. Simulation Studies of Self-Assembly of End-Tethered Nanorods in Solution and Role of Rod Aspect Ratio and Tether Length. *J. Chem. Phys.* **2006**, *125*, 184903.
79. Bray, A. J. Theory of Phase Ordering Kinetics. *Adv. Phys.* **1994**, *43*, 357–459.
80. Nagle, J. F. Area per Lipid of Lipid Bilayers from NMR. *Biophys. J.* **1993**, *64*, 1476–1481.
81. Lague, P.; Zuckermann, M. J.; Roux, B. Protein Inclusion in Lipid Membranes: A Theory on the Hypernetted Chain Integral Equation. *Faraday Discuss* **1998**, *111*, 165–172.
82. Lague, P.; Zuckermann, M. J.; Roux, B. Lipid-Mediated Interactions bBetween Intrinsic Membrane Proteins: A Theoretical Study Based on Integral Equations. *Biophys. J.* **2000**, *79*, 2867–2979.
83. Lague, P.; Zuckermann, M. J.; Roux, B. Lipid-Mediated Interactions between Intrinsic Membrane Proteins: Dependence on Protein Size and Lipid Composition. *Biophys. J.* **2001**, *81*, 276–284.
84. May, S.; Ben-Shaul, A. A Molecular Model for Lipid-Mediated Interaction between Proteins in Membranes. *Phys. Chem. Chem. Phys.* **2000**, *2*, 4494–4502.
85. Plimpton, S. Fast Parallel Algorithms for Short-Range Molecular Dynamics. *J. Comput. Phys.* **1995**, *117*, 1–19; http://lammps.sandia.gov/cite.html.